



This is a repository copy of *Effect of airgap length on electromagnetic performance of permanent magnet Vernier machines with different power ratings.*

White Rose Research Online URL for this paper:

<https://eprints.whiterose.ac.uk/178625/>

Version: Accepted Version

Article:

Kana Padinharu, D.K., Li, G.-J., Zhu, Z.Q. et al. (3 more authors) (2022) Effect of airgap length on electromagnetic performance of permanent magnet Vernier machines with different power ratings. *IEEE Transactions on Industry Applications*, 58 (2). pp. 1920-1930. ISSN 0093-9994

<https://doi.org/10.1109/TIA.2021.3135256>

© 2021 IEEE. Personal use of this material is permitted. Permission from IEEE must be obtained for all other users, including reprinting/ republishing this material for advertising or promotional purposes, creating new collective works for resale or redistribution to servers or lists, or reuse of any copyrighted components of this work in other works. Reproduced in accordance with the publisher's self-archiving policy.

Reuse

Items deposited in White Rose Research Online are protected by copyright, with all rights reserved unless indicated otherwise. They may be downloaded and/or printed for private study, or other acts as permitted by national copyright laws. The publisher or other rights holders may allow further reproduction and re-use of the full text version. This is indicated by the licence information on the White Rose Research Online record for the item.

Takedown

If you consider content in White Rose Research Online to be in breach of UK law, please notify us by emailing eprints@whiterose.ac.uk including the URL of the record and the reason for the withdrawal request.



eprints@whiterose.ac.uk
<https://eprints.whiterose.ac.uk/>

Effect of Airgap Length on Electromagnetic Performance of Permanent Magnet Vernier Machines with Different Power Ratings

D. K. Kana Padinharu, G. J. Li, Z. Q. Zhu, Z. Azar, R. Clark, and A. Thomas

Abstract – This paper investigates the effect of airgap length on the electromagnetic performance of direct-drive surface mounted permanent magnet Vernier (SPM-V) machines with different power ratings. Using 3kW machine as an example, its performance is comprehensively compared with a conventional surface mounted permanent magnet (SPM) machine with the same airgap lengths using 2D Finite Element Analysis (FEA). For each airgap length, the slot/pole number combination for the SPM-V machine is investigated to achieve the optimal performance compared to the conventional SPM machine. In order to make the study more generic, the slot/pole number and the airgap length variations are expressed as normalized pole pitch, i.e. $\bar{\tau}_r$ (ratio of rotor pole pitch to electromagnetic airgap length). The results show that for 3kW machines, $\bar{\tau}_r > 2.2$ is a good design criterion for the SPM-V machines to achieve higher average torque and efficiency than the conventional SPM machines. In addition, a reasonably good power factor (>0.9 in this case) can be achieved. Although the power factor of SPM-V machines drops significantly at multi-MW power level, i.e. 3MW and 10MW, the criterion $\bar{\tau}_r > 2.2$ still results in achieving a performance closest to their optimal capability. However, when $\bar{\tau}_r > 2.2$, special consideration should be paid to avoid potential irreversible magnet demagnetization at multi-MW power levels.

Index Terms—Airgap permeance, demagnetization, efficiency, leakage flux, power factor, Vernier machine.

I. INTRODUCTION

Direct-drive machines are gaining popularity in applications such as electric vehicles [1], [2], offshore-wind power generation [3], etc. Direct-drive technology makes the drivetrain system much simpler and reliable by eliminating the requirement of gearboxes or any mechanical transmission between the machine and the load. However, the high torque requirement at low speed makes these direct-drive machines very bulky and costly. Different permanent magnet machine topologies have been proposed to reduce the size and weight of direct-drive machines such as transverse flux [4], [5], axial field [6], [7] and magnetically geared machines [7], [8]. However, these proposed machines either have a complex 3D structure or have multiple airgaps which makes them difficult to manufacture.

In the recent decade, Vernier machines have become very popular because of their simple structure (similar to conventional SPM machines) and high torque density. Vernier machines work on the principle of flux modulation/magnetic gearing effect which makes them inherently favorable for direct-drive multi-pole topologies. Different direct-drive Vernier machines have been proposed in literature to improve their torque density. A 2.2kW outer rotor permanent magnet Vernier machine with split teeth stator has been proposed in [9] for direct-drive wind power

generation. The design adopts an airgap length of 0.6mm at 150rpm with machine outer diameter of 233mm. Similarly, an outer rotor Vernier machine with magnets on both sides of the rotor and the stator is discussed in [10] for in-wheel motor application. This machine is designed with a 2mm airgap length for a 180mm machine outer diameter (150rpm speed). A linear Vernier machine with a modular structure having a 1.5mm airgap length has been proposed in [11] to minimize the force ripple for direct-drive servo applications. In general, the above-mentioned references discuss the high torque density capability of Vernier machines for different direct-drive applications. It is also noted that Vernier machines with similar outer diameters can be designed with different airgap lengths and slot/pole number combinations according to the specific applications and design requirements.

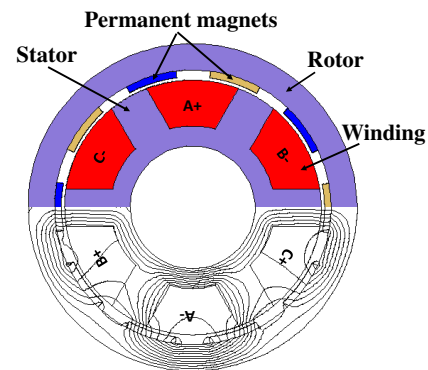


Fig. 1. Schematic and open-circuit flux distribution of an outer rotor SPM-V machine with slot/pole number $Z = 6$, $P_r = 5$ and $P_s = 1$ [12]. Z is the number of stator slots, P_r is the rotor pole pair number and P_s is the stator winding pole pair number. Yellow and blue colours of the magnets indicate opposite magnetization polarity.

Although the smallest possible airgap length would be favorable for better electromagnetic performance, a few factors are limiting the choice of airgap length for Vernier machines. For example,

- a smaller airgap length increases the manufacturing complexity and hence the cost of the machine. As a thumb rule, an airgap length of 0.1% of the airgap diameter is often chosen for direct-drive wind power generators [13]. Therefore, it is important to investigate the influence of airgap length for PM Vernier machines with different power ratings.
- the slot/pole number combination for the minimum possible airgap length needs to be carefully chosen to maximize the performance. This is done by choosing the right normalized pole pitch value.
- Vernier machines have a high risk of irreversible demagnetization at high power levels [14]. Hence the high performance achieved by using a small airgap length may

not be suitable from a demagnetization withstand capability point of view.

However, to date, there have been no studies showing how to select the appropriate slot/pole number combinations for a specific airgap length to achieve optimal performance for the Vernier machines. In most cases, an iterative method is adopted to optimize the design for a given airgap length by varying the slot/pole number combinations [14]–[16]. However, this approach is design specific and will have to be repeated on a case-by-case basis. Moreover, the performance factors such as average torque, torque ripple, power factor and efficiency, etc. of Vernier machines are very sensitive to the airgap permeance which is a function of airgap length and slot/pole number combinations [14], [17]. Hence, it would be useful to develop a generic criterion about the selection of airgap length and slot/pole number combination. The novelty and contribution of this paper are the proposal of such a generic criterion that can be applied in the design phase of Vernier machines to achieve an overall good performance, especially in comparison with their conventional SPM counterparts. This requires a systematic study of the performance of SPM-V machines in comparison with conventional SPM machines for different airgap lengths, slot/pole number combinations and a wide range of power levels, i.e. 3kW, 3MW and 10MW, which has not been reported in the literature. This paper is an extension of the original work presented in [18]. An outer rotor topology, for example, the schematic shown in Fig. 1, will be considered for this study as it is more favorable for direct-drive applications. It is worth noting that the FE models used for the analyses in this paper have been validated by experiments in [12], which provides good confidence in the numerical results obtained.

II. IMPORTANCE OF AIRGAP PERMEANCE IN SPM-V MACHINES

As mentioned previously, SPM-V machines work on the principle of airgap flux modulation. The working principle of Vernier machines utilizing fundamental and modulated airgap flux density harmonics has been widely discussed in the literature [15], [16], [19]. To utilize this modulated airgap flux density component and to maximize the torque capability in an SPM-V machine, the slot/pole number combination follows the rule [20]

$$P_s = Z - P_r \quad (1)$$

where Z is the number of stator slots, P_r is the rotor pole pair number and P_s is the stator winding pole pair number. For example, an SPM-V machine with $Z = 6$ and $P_s = 1$ will have a rotor with 5 pole pairs of rotor magnets. However, a conventional machine with the same stator structure will only have 1 rotor pole pair. By adopting such a slot/pole number combination, the Vernier machines develop high tangential airgap flux density and thereby much higher torque than their conventional counterparts [21]. However, the high rotor pole pairs result in high inter-pole leakage fluxes and thereby poor power factors.

The induced EMF (E_{ph-v}) of the SPM-V machines can be represented in terms of the airgap flux density harmonics as [16]

$$E_{ph-v} = \frac{k_w T_{ph} \omega_m D_g L_{stk}}{\sqrt{2}} \left(G_r B_{Z-P_r} + B_{P_r} + \frac{P_r}{(Z + P_r)} B_{Z+P_r} \right) \quad (2)$$

where k_w is the fundamental winding factor, T_{ph} is the number of series turns per phase, ω_m is the rotor mechanical angular velocity, D_g and L_{stk} are the airgap diameter and the stack length, respectively. The fundamental (B_{P_r}) and modulated (B_{Z-P_r} , B_{Z+P_r}) airgap flux densities are generated by the interaction between the fundamental MMF of the rotor permanent magnets and the airgap permeance. G_r is the gear ratio of the Vernier machine defined as the ratio of rotor pole number (P_r) to stator winding pole pair number (P_s).

The induced EMF can be further represented in terms of airgap permeance coefficients and gear ratio as [12]

$$E_{ph-v} = \frac{k_w T_{ph} \omega_m D_g L_{stk} B_{P_r}}{\sqrt{2}} \left(\frac{G_r^2}{(2G_r + 1)} \Lambda_r + 1 \right) \quad (3)$$

where Λ_r is the relative airgap permeance defined as the ratio of the fundamental (Λ_1) to the DC (Λ_0) component of the airgap permeance function. For the comparative study of induced EMF for different airgap lengths, the per-unit EMF (E_{PU}) term is introduced as

$$E_{PU} = \frac{E_{ph-v}}{E_{ph-c}} \quad (4)$$

where E_{ph-c} is the phase back-EMF of the conventional SPM machine.

For an SPM-V machine designed with the same machine parameters as the conventional SPM machine, E_{PU} is

$$E_{PU} = \left(\frac{G_r^2}{(2G_r + 1)} \Lambda_r + 1 \right) = K_{ver} + 1 \quad (5)$$

where $K_{ver} = \frac{G_r^2}{(2G_r + 1)} \Lambda_r$, is the Vernier factor which is the extra EMF component generated in an SPM-V machine, which does not exist in a conventional SPM machine. From (5), it can be found that the induced EMF of the SPM-V machine, for a given gear ratio (G_r), is largely a function of the relative airgap permeance (Λ_r). Hence it is important to study the trend of Λ_r with different airgap lengths and slot/pole numbers which will be discussed in section IV.

III. 2D FINITE ELEMENT MODELLING

As an example, 3kW power rating is selected for the following analyses. The 2D FEA model for one coil pitch of the 3kW conventional SPM machine with an outer rotor topology is shown in Fig. 2(a). Its key parameters are given in TABLE I. The airgap length is varied from 1mm to 5mm in increments of 1mm.

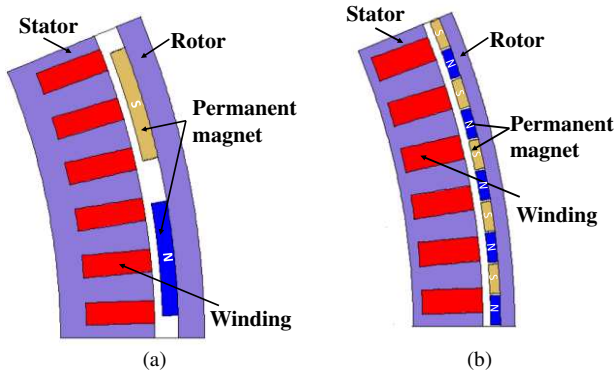


Fig. 2. Comparison of 2D models (one pole pair). (a) conventional SPM machine and (b) SPM-V machine.

It is worth noting that the 3kW direct-drive machine discussed in this paper is a small-scale prototype design originally developed for wind power applications. Hence, the design incorporates some of the design features generally adopted in large power direct-drive wind generators. For example, the aspect ratio (ratio of stack length to airgap diameter) is 0.25, a relatively large airgap length of 2mm, a terminal voltage of 690V, etc. Assuming natural air cooling, the current density for this machine is limited to $3.7\text{A}/\text{mm}^2$. These design rules have resulted in a relatively low electrical loading of $8.6\text{AT}/\text{mm}$.

The SPM-V machine shown in Fig. 2(b) is derived from the conventional SPM machine by changing the slot/pole number which follows the rule given in (1). It has been observed that the power factor of SPM-V machines significantly reduces with higher electrical loadings/power ratings [22]. The maximum value achieved is around 0.4-0.5 for multi-MW direct-drive SPM-V machines designed with $G_r=5$. A higher G_r can result in even lower power factor. Therefore, a $G_r=5$ is chosen for this study which is the minimum G_r possible to realize a single-layer winding desirable for high power machines. For each airgap length, the slot/pole number combination of the SPM-V machine is varied (with $G_r=5$) to evaluate the optimal performance. The different slot/pole number combinations used in this study for the SPM-V machine are given in TABLE II.

TABLE I KEY PARAMETERS OF SPM MACHINE

Rated power (kW)	3	Magnet volume (m^3)	0.000408
Rated speed (rpm)	170	Magnet B_r, μ_r	1.23, 1.02
Stack length (mm)	110	Phase current (Arms)	2.5
Airgap length (mm)	1,2,3,4,5	Turns/phase	720
Rotor outer diameter (mm)	426.4	Electrical loading (AT/mm)	8.6

TABLE II SLOT/POLE NUMBER COMBINATIONS

Machine type	Z	P_r	P_s	LCM (Z, $2P_r$)
Conventional	96	16	16	96
Vernier	36	30	6	180
Vernier	48	40	8	240
Vernier	72	60	12	360
Vernier	96	80	16	480
Vernier	120	100	20	600

Note: LCM is the least common multiple.

All the designs for both the conventional SPM and SPM-V machines are globally optimized for achieving maximum torque capability. It is worth noting that during the optimization process, all the dimensions shown in TABLE I are maintained the same for the two machines when they have different airgap lengths. This will inevitably lead to different output powers as will be investigated in the following

sections. However, in order to maintain the same thermal performance between the two machines, the copper loss has been kept the same.

IV. COMPARISON FOR DIFFERENT AIRGAP LENGTHS

A. Induced EMF

According to (5), for a given gear ratio G_r , the per unit induced EMF (E_{PU}) is directly proportional to Λ_r . The value of Λ_r computed using 2D FEA [23] for different airgap lengths across different slot/pole numbers for the SPM-V machine is shown in Fig. 3. It can be observed that for a given slot/pole number, Λ_r decreases with increase in airgap length. Similarly, for a given airgap length, Λ_r decreases with an increase in pole number.

The E_{PU} predicted using 2D FEA shows a similar trend like Λ_r as shown in Fig. 4. For small airgap lengths, the SPM-V machine generally outperforms the conventional SPM machine for the wide range of slot/pole numbers considered. The maximum induced EMF achieved is at 1mm airgap length and is almost 1.62 times that of the conventional SPM machines. However, with the increase in airgap length, the choice of slot/pole numbers for the SPM-V machines which can achieve higher EMF than the conventional SPM counterparts is limited.

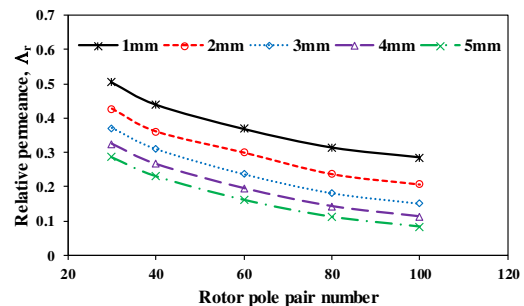


Fig. 3. Comparison of Λ_r predicted using 2D FEA [23] for different airgap lengths across all slot/pole numbers of the SPM-V machines.

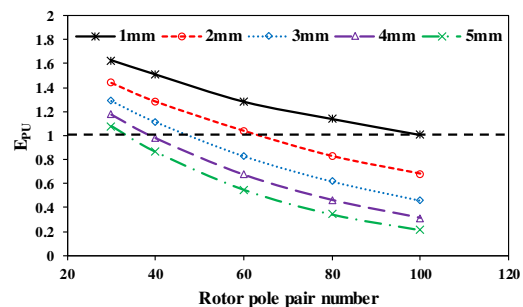


Fig. 4. Comparison of E_{PU} predicted directly using 2D FEA for different airgap lengths across all slot/pole numbers of the SPM-V machines.

The low EMF values of the SPM-V machines at higher pole numbers and larger airgap lengths are due to their high inter-pole leakage fluxes. The comparison of open circuit flux distribution at 5mm airgap length between the conventional SPM machine with $N_s=96, P_r=16$ and the SPM-V machine with $N_s=96, P_r=80, P_s=16$ over one coil pitch is shown in Fig. 5. Even at an airgap length of 5mm, the inter-pole leakage flux for the conventional SPM machine is negligible compared to the flux per pole. However, for the SPM-V machine, almost all the fluxes of the 5 magnets under one coil pitch can be regarded as leakage fluxes.

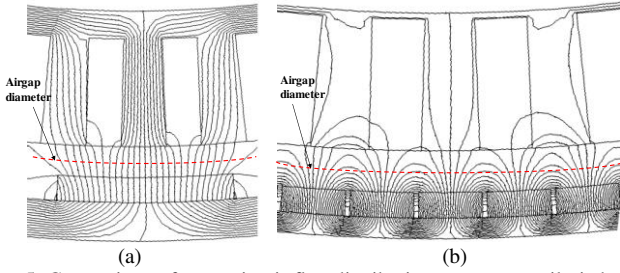


Fig. 5. Comparison of open-circuit flux distributions over one coil pitch at an airgap length of 5mm. (a) conventional SPM machine with $N_s = 96, P_r = 16$ and (b) SPM-V machine with $N_s = 96, P_r = 80, P_s = 16$.

B. Average Torque and Torque Ripple

As mentioned in section III, the phase current is maintained the same for different airgap lengths across all slot/pole numbers of SPM-V machines. Therefore, the torque performance is expected to largely follow the induced EMF trend unless the machine has reached magnetic saturation. Similar to induced EMF, the per-unit torque ($Torque_{PU}$) is introduced to compare the performance of SPM-V machine against the conventional SPM machine. The $Torque_{PU}$ comparison for different airgap lengths across all slot/pole numbers of the SPM-V machines is shown in Fig. 6. As expected, the torque performance is similar to the induced EMF as the impact of saturation is not significant.

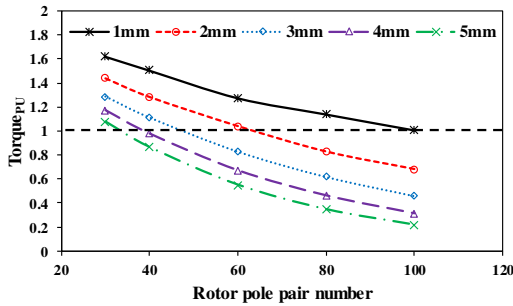


Fig. 6. Comparison of $Torque_{PU}$ predicted directly using 2D FEA for different airgap lengths across all slot/pole numbers of the SPM-V machine.

In order to make the study more generic and useful for the SPM-V machine design, the slot/pole numbers with different airgap lengths are represented as normalized pole pitch ($\bar{\tau}_r$) defined as [12]

$$\bar{\tau}_r = \frac{\tau_r}{g + \frac{h_m}{\mu_{rec}}} \quad (6)$$

where τ_r is the rotor pole pitch, g is the mechanical airgap length, h_m and μ_{rec} are the magnet thickness and recoil permeability.

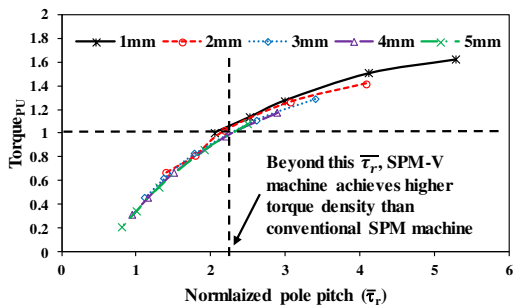
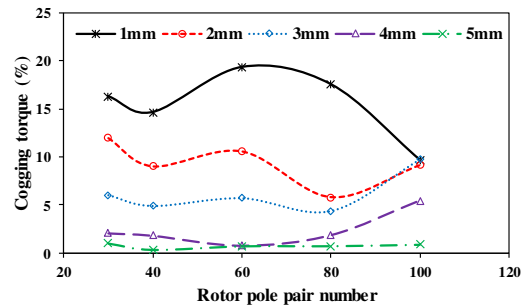


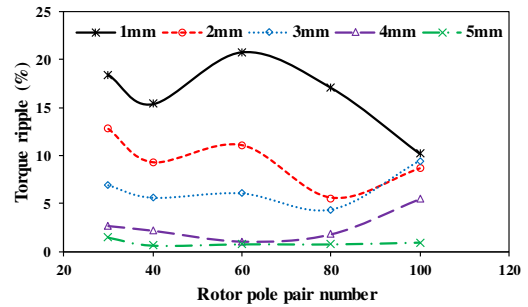
Fig. 7. Comparison of $Torque_{PU}$ predicted directly using 2D FEA as a function of normalized pole pitch ($\bar{\tau}_r$) of the SPM-V machine.

$Torque_{PU}$ as a function of $\bar{\tau}_r$ is shown in Fig. 7. It can be observed that $Torque_{PU}$ is clearly a function of $\bar{\tau}_r$ with all the torque curves almost overlapping each other. The study shows that for a 3kW power rating, the SPM-V machine designed around a $\bar{\tau}_r > 2.2$ can achieve higher torque density than the conventional counterpart.

The comparison of the cogging torque $[(CT_{max} - CT_{min})/T_{av} \times 100\%]$, where CT_{max} , CT_{min} are the maximum, the minimum values of cogging torque and T_{av} is the average on-load torque during one electrical period] for different airgap lengths across all slot/pole numbers of the SPM-V machines is shown in Fig. 8(a). Whereas the cogging torques for the conventional SPM machine are given in TABLE III. It is observed that SPM-V machines in general have low cogging torque compared to conventional SPM machines and the reason is as follows. The Least Common Multiple (LCM) between Z and $2P_r$ for the SPM-V machine is found to be higher than that of the conventional SPM machine as highlighted in TABLE II. It is generally true that the higher the value of LCM, the lower the cogging torque [24].



(a)



(b)

Fig. 8. Comparison of (a) cogging torque and (b) torque ripple for different airgap lengths across all slot/pole numbers of the SPM-V machines.

TABLE III COGGING TORQUE AND TORQUE RIPPLE VALUES OF THE CONVENTIONAL SPM MACHINES

Parameter	Airgap length(mm)				
	1	2	3	4	5
Cogging torque (%)	304	165.8	69	5.3	29
Torque ripple (%)	305	166.5	69	9.6	30

In general, for the conventional SPM machine with integer slot winding (slots/pole/phase=1), different cogging torque reduction techniques such as magnet shaping, skewing, etc. can be adopted. However, for this analysis, these techniques are not incorporated in the model to have a fair comparison with the SPM-V machine. Moreover, since the global optimization was performed for maximizing the torque performance, the cogging torque may not be optimal for conventional SPM and therefore shows a relatively high value. As can be expected, cogging torque is found to be decreasing with the increase in airgap length for both

machines. However, for a given airgap length, there is no specific trend observed across slot/pole numbers of the SPM-V machines.

The on-load torque ripple $[(T_{max}-T_{min})/T_{av}\times 100\%$, where T_{max} and T_{min} are the maximum and the minimum values of on-load torque during one electrical period] for different airgap lengths across all slot/pole numbers of the SPM-V machines are shown in Fig. 8(b). It is observed that for both machines, as mentioned previously, the torque ripple is largely dominated by the cogging torque. Hence, the torque ripple shows a similar trend as the cogging torque.

C. Power Factor

Vernier machines are known for their relatively poor power factor compared to conventional PM machines [25], [26]. The comparison of power factors (at rated load) for different airgap lengths across all slot/pole numbers of the SPM-V machines is shown in Fig. 9.

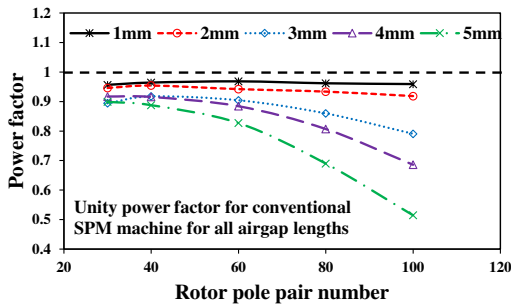


Fig. 9. Comparison of power factor predicted directly using 2D FEA for different airgap lengths across all slot/pole numbers of the SPM-V machines.

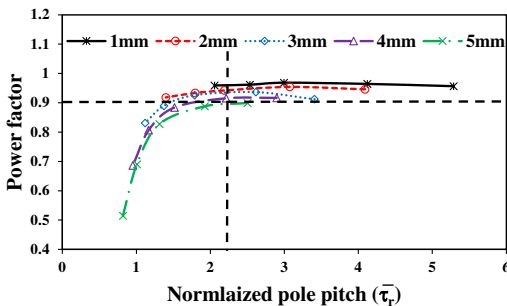


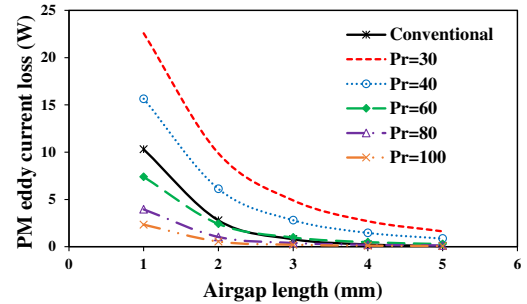
Fig. 10. Comparison of power factor predicted directly using 2D FEA as a function of $(\bar{\tau}_r)$ of the SPM-V machine.

The power factors for the conventional SPM machines are found to be almost unity for all the airgap lengths. However, for the SPM-V machine, there is a significant drop in power factor with an increase in airgap length, especially for higher pole numbers. The maximum power factor achievable for the SPM-V machine is 0.97 at 1mm airgap length (with an electrical loading of 8.35AT/mm) and the minimum value is 0.51 at 5mm airgap length. This drop in power factor for the SPM-V machines is due to high inter-pole leakage at high slot/pole numbers as shown in Fig. 5(b). The power factor as a function of $\bar{\tau}_r$ shown in Fig. 10 reveals that a value greater than 0.9 is achievable with $\bar{\tau}_r > 2.2$ at 3kW power level.

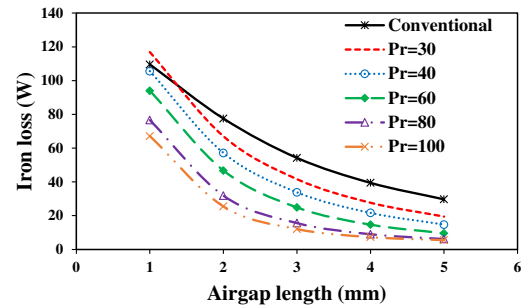
D. Electromagnetic Losses and Efficiency

For the calculation of efficiency, electromagnetic losses such as PM eddy current, copper, stator and rotor iron losses are considered. As the rotor speed and the speed of the fundamental armature MMF are asynchronous, the PM eddy current losses are generally found to be high in Vernier machines [27]. To limit the PM eddy current loss, 2

circumferential PM segmentations are employed for each pole in both the SPM-V and conventional SPM machines. The comparison of PM eddy current losses for different airgap lengths between the conventional SPM machines and SPM-V machines (with different slot/pole numbers) is shown in Fig. 11(a). As expected, the PM eddy current losses significantly drop with increasing airgap length for both types of machines. As mentioned above, the main source of PM eddy current loss in Vernier machine is the fundamental armature flux. Due to high slot leakage flux at high slot/pole numbers, the proportion of armature flux linking with PMs is much lower than that with lower slot/pole numbers. Moreover, with relatively large PM width, the eddy current losses in Vernier machines with lower slot/pole number are much higher than that with high slot/pole numbers.



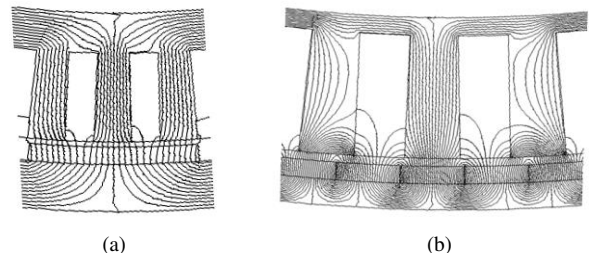
(a)



(b)

Fig. 11. Comparison of losses using 2D FEA for different airgap lengths across all slot/pole numbers of the SPM-V machines. (a) PM eddy current loss and (b) iron loss.

The comparison of stator and rotor iron losses for different airgap lengths between the conventional SPM and SPM-V machines (with different slot/pole numbers) is shown in Fig. 11(b). Since the electrical loading of the chosen 3kW machine is relatively low, the iron loss is mainly dominated by the PM flux. Unlike the conventional SPM machines, the inter-pole PM leakage flux in the SPM-V machines is very sensitive to the airgap length and increases significantly with increasing airgap length and towards high pole number.



(a)

(b)

Fig. 12. Comparison of open-circuit flux distributions over one coil pitch for an airgap length of 1mm. (a) Conventional SPM machine with $N_s = 96, P_r = 16$. (b) SPM-V machine with $N_s = 96, P_r = 80, P_s = 16$.

This can be confirmed by comparing the open-circuit flux distributions with 1mm (see Fig. 12) and 5mm (see Fig. 5)

airgap lengths for the conventional SPM and SPM-V machines. Because of these reasons the iron losses in the SPM-V machines are found to reduce at a faster rate with increasing airgap length. Due to high PM leakage fluxes, the SPM-V machines exhibit lower iron losses than the conventional SPM machines.

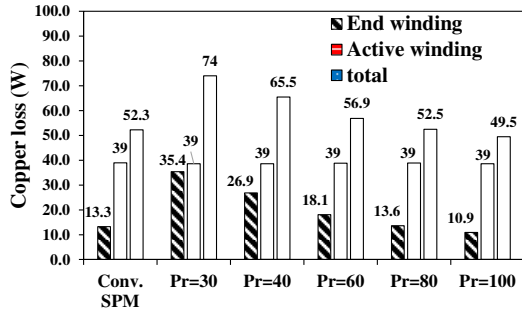


Fig. 13. Comparison of copper losses (active and end windings) between the conventional SPM and SPM-V machines with different slot/pole number combinations.

The copper losses for the active and end windings are compared between the conventional SPM and SPM-V machines with different slot/pole numbers in Fig. 13. Although the copper loss of the active winding is maintained constant across different machines, the copper loss of the end winding increases towards lower pole numbers for the SPM-V machines due to their longer end winding length.

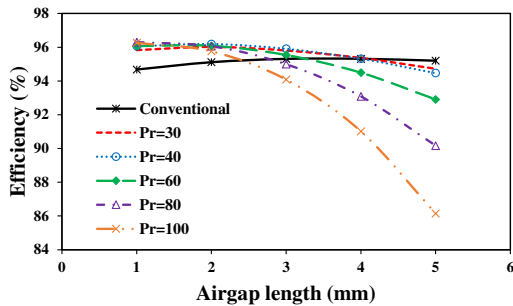
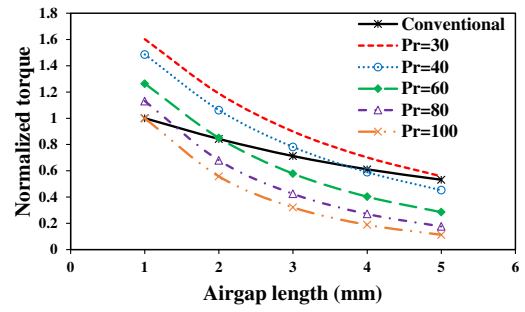


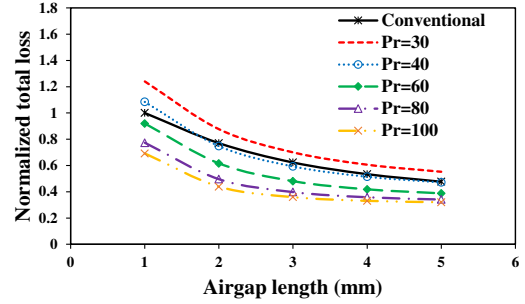
Fig. 14. Comparison of efficiencies for different airgap lengths between the conventional SPM and SPM-V machines with different slot/pole numbers.

The comparison of the efficiencies for different airgap lengths between the conventional SPM and SPM-V machines with different slot/pole numbers is shown in Fig. 14. It is interesting to note that the efficiency of the conventional SPM machines is slightly increasing towards larger airgap lengths. However, there is a significant drop in efficiency for the SPM-V machines towards larger airgap lengths and larger pole numbers. This can be explained as follows.

The variation of efficiency with airgap length will depend on the change rate of average torque and total electromagnetic losses. For the conventional SPM machines, the rate of decrease of average torque with increasing airgap length is similar to the rate of decrease of electromagnetic losses, as shown in Fig. 15. Hence, the conventional SPM machines can maintain almost constant efficiency for different airgap lengths. However, for the SPM-V machines, the rate of decrease of average torque with increasing airgap length is larger than that of electromagnetic losses, especially towards larger pole numbers. This results in a significant drop in efficiency for larger pole numbers and longer airgap lengths. At shorter airgap lengths, as the normalized torque of the SPM-V machines is higher than the normalized total electromagnetic loss, they can achieve higher efficiency than the conventional SPM machines.



(a)



(b)

Fig. 15. Comparison of (a) normalized average torque (b) normalized total electromagnetic losses for different airgap lengths between the conventional SPM and SPM-V machines with different slot/pole numbers. The conventional SPM machine with 1mm airgap length is taken as reference for the calculation of normalized values.

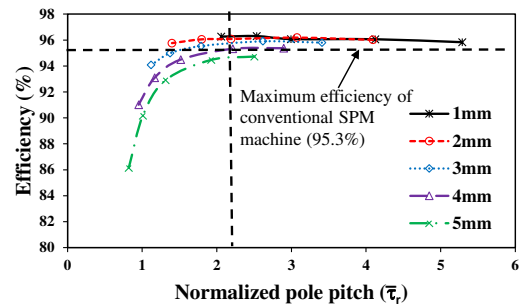


Fig. 16. Comparison of efficiency as a function of $\bar{\tau}_r$ for the SPM-V machines with different airgap lengths.

The efficiency as a function of $\bar{\tau}_r$ is shown in Fig. 16. It can be observed that at $\bar{\tau}_r > 2.2$, the efficiency of the SPM-V machines is comparable to or greater than the conventional SPM machines.

E. Demagnetization

It has been found in [14] that at MW power levels, the SPM-V machines are more susceptible to irreversible demagnetization, especially towards lower pole numbers (higher $\bar{\tau}_r$ values). Hence, demagnetization analysis would be critical for obtaining a desirable range of $\bar{\tau}_r$ that ensures the SPM-V machines to achieve both optimal performance and good demagnetization withstand capability. The demagnetization analysis is performed under a 3-phase symmetrical short circuit fault and the approach is similar to that in [14]. The results showed that both the conventional SPM and SPM-V machines do not have any irreversible demagnetization for the entire range of airgap lengths investigated across all the slot/pole number combinations. This is mainly due to the low electrical loading at the 3kW power range.

F. SPM-V Machines with Higher Gear Ratios

The performance of SPM-V machines is also sensitive to the designed gear ratios. It has been observed that the SPM-V machines designed with a gear ratio of 5 have already a very low power factor (~ 0.4 - 0.5) at multi-MW power ratings due to their high electrical loadings [22]. Hence, a higher gear ratio will only worsen the power factor and may not be suitable for high power ratings. However, for small power ratings in the range of few kW, higher gear ratios can be considered for achieving higher torque density and reasonably good power factor. Hence, it would be valuable to investigate the right choice of $\bar{\tau}_r$ for SPM-V machines designed with higher gear ratios. As an example a $G_r = 11$ is chosen that is widely used in literature [16], [28], [29]. Selecting the same range of stator slots as shown in TABLE II, the slot/pole number combinations investigated with $G_r = 11$ are given in TABLE IV. The airgap length for each slot/pole number combination is varied from 1mm to 5mm with an increment of 1mm. The analysis approach adopted is the same as that with $G_r = 5$.

TABLE IV SLOT/POLE NUMBER COMBINATIONS

Machine type	Z	P_r	P_s
Conventional	96	16	16
Vernier	36	33	3
Vernier	48	44	4
Vernier	72	66	6
Vernier	96	88	8
Vernier	120	110	10

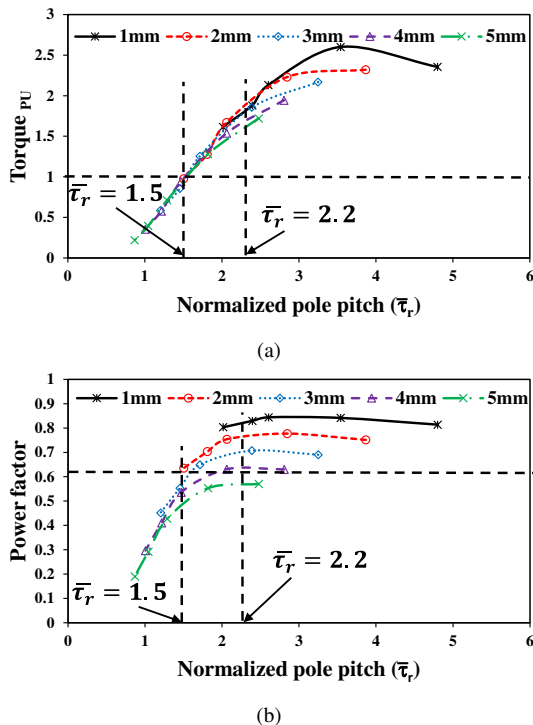


Fig. 17. $Torque_{pu}$ and power factor as a function of normalized pole pitch ($\bar{\tau}_r$) for the SPM-V machines with $G_r = 11$. (a) $Torque_{pu}$. (b) Power factor.

The $Torque_{pu}$ and power factor of the investigated machines with $\bar{\tau}_r$ are shown in Fig. 17. Unlike $G_r = 5$, the SPM-V machines with $G_r = 11$ can achieve a torque higher than the conventional SPM machines at around $\bar{\tau}_r = 1.5$. However, the power factor is very low, i.e. in the range of ~ 0.45 - 0.6 , at this $\bar{\tau}_r$. This range of power factors may be acceptable for multi-MW power ratings where the direct-drive machines are bulkier and more expensive than the power converters. The high torque density of the generator

can offset the increased cost of the power converter, achieving an overall competitive system level cost compared to the conventional SPM machines [30]. However, for small power ratings, a higher power factor is desirable and in this case, it is achieved for $\bar{\tau}_r > 2.2$.

Hence, $\bar{\tau}_r > 2.2$ can be a good design criterion for the SPM-V machines (few kW range) in achieving a reasonably good performance in comparison with the conventional SPM machines. However, with the increasing popularity of direct-drive PM machines in high power (multi-MW) applications, it is important to verify the validity of this conclusion for those power levels as well.

V. EXTENDING THE STUDY TO MULTI-MW POWER LEVEL

For this investigation, two direct-drive outer rotor conventional SPM machines, i.e. 3MW [31] and 10MW [13], have been selected [22]. The key parameters of these machines are listed in TABLE V. Although these machines were originally designed for inner rotor topology, they have been converted to an outer rotor topology and then globally optimized for maximum torque. It is worth noting that these optimized conventional SPM designs have been used for a comprehensive comparison against the SPM-V machines in [12], [14], [22], [30].

TABLE V KEY PARAMETERS OF 3MW AND 10MW CONVENTIONAL SPM MACHINES

Parameters	3 MW	10 MW
Rated speed (rpm)	15	10
Outer diameter (m)	5	10
Airgap length (mm)	3,4,5,6,7	6,8,10,12,14
Stack length (m)	1.2	1.8
Magnet volume (m ³)	0.227	0.92
Phase current (Arms)	2694	8796
Electrical loading (AT/mm)	59	54.5
Turns/phase	56	32

The methodology adopted for deriving the slot/pole number combinations of the SPM-V machines and their optimization is the same as those of the 3kW machines investigated in previous sections. The different slot/pole number combinations for the SPM-V machines are shown in TABLE VI. Due to the poor power factor of the SPM-V machines at high electrical loadings/power ratings, the analysis is limited to $G_r = 5$.

TABLE VI SLOT/POLE NUMBER COMBINATIONS FOR 3MW AND 10MW CONVENTIONAL SPM AND SPM-V MACHINES

Machine type	3MW			10MW		
	Z	P_r	P_s	Z	P_r	P_s
Conventional	480	80	80	960	160	160
Vernier	120	100	20	120	100	20
Vernier	192	160	32	240	200	40
Vernier	240	200	40	360	300	60
Vernier	360	300	60	480	400	80
Vernier	480	400	80	960	800	160

The 3MW and 10MW conventional SPM machines are originally designed with an airgap length of 5mm and 10mm, respectively. However, for studying the influence of airgap length, their values are varied in increments of 1mm and 2mm for the 3MW and 10MW, respectively, as shown in TABLE V.

A. Average Torque and Torque Ripple

The $Torque_{pu}$ as a function of $\bar{\tau}_r$ for both 3MW and 10MW SPM-V machines are shown in Fig. 18.

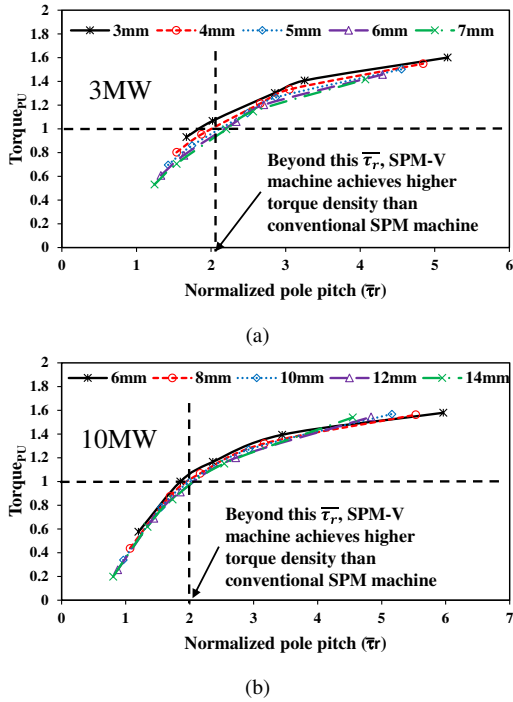


Fig. 18. $Torque_{pU}$ as a function of normalized pole pitch ($\bar{\tau}_r$) for the SPM-V machines. (a) 3MW. (b) 10MW.

The torque ripple for the 3MW and 10MW SPM-V machines with different airgap lengths are shown in Fig. 19. As expected, the torque ripple reduces with increasing airgap length for both the SPM-V and conventional SPM machines (see TABLE VII). Similar to the 3kW machines, the torque ripple of the SPM-V machines is lower than those of the conventional SPM machines with the same airgap length. It is observed that for both machines, the torque ripple is largely determined by the cogging torque.

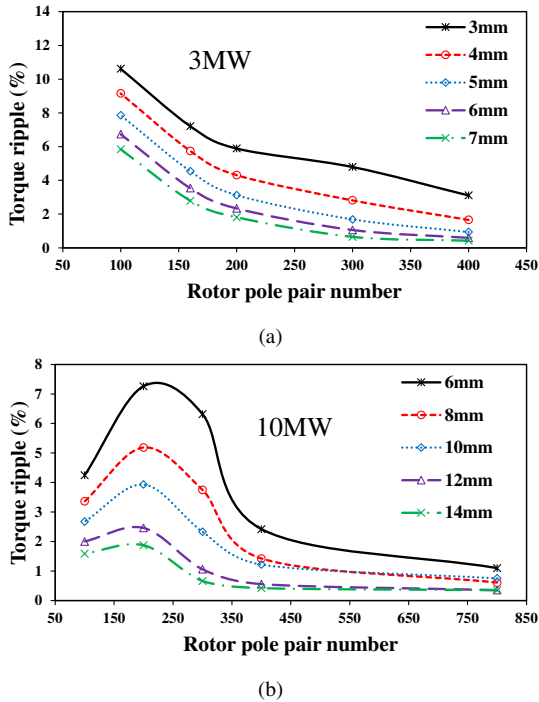


Fig. 19. Comparison of torque ripples for different airgap lengths across all slot/pole numbers of the SPM-V machines. (a) 3MW. (b) 10MW.

B. Power Factor

The trends of power factor as a function of $\bar{\tau}_r$ for both the 3MW and 10MW SPM-V machines are shown in Fig. 20.

Firstly, the maximum power factors at these power levels are observed to be significantly lower (~ 0.1 - 0.55) compared to the 3kW machines. Whereas the conventional SPM machines still have a good power factor (~ 0.92 - 0.95) as shown in TABLE VII. The reason for the low power factor of the SPM-V machines at high power levels is ascribed to the high electrical loading combined with the gearing effect [22].

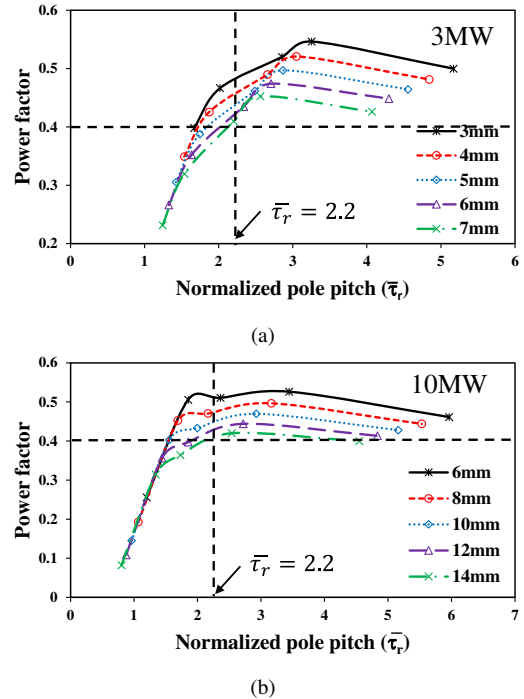


Fig. 20. Power factor as a function of normalized pole pitch ($\bar{\tau}_r$) for SPM-V machines. (a) 3MW. (b) 10MW.

TABLE VII PERFORMANCE OF 3MW AND 10MW CONVENTIONAL SPM MACHINES WITH DIFFERENT AIRGAP LENGTHS

3MW					
Airgap length (mm)	3	4	5	6	7
Torque ripple (%)	56.1	47.5	40.2	34	29
Power factor	0.95	0.94	0.94	0.93	0.92
Efficiency (%)	97.37	97.37	97.36	97.33	97.29
10MW					
Airgap length (mm)	8	9	10	11	12
Torque ripple (%)	26.2	21.75	18.1	14.9	12.4
Power factor	0.96	0.95	0.95	0.94	0.94
Efficiency (%)	97.96	97.95	97.94	97.92	97.9

Secondly, the SPM-V machines show a significant drop in power factor with increasing airgap length. However, for conventional SPM machines, the decrease in power factor due to increasing airgap length is negligible as shown in TABLE VII. Similar to the 3kW SPM-V machines, the power factor is observed to be significantly reduced for the 3MW and 10MW power levels when $\bar{\tau}_r < 2.2$. However, although the power factor is low, the criterion $\bar{\tau}_r > 2.2$ can still help these MW level SPM-V machines to achieve a power factor closest to its maximum values.

C. Efficiency

To limit the PM eddy current loss (in addition to the 2 circumferential segmentations), both the conventional SPM and SPM-V machines at 3MW and 10MW have 26 and 40 axial segments, respectively. The axial segmentation effect on PM eddy current loss is estimated using a correction factor calculated in [32]. The efficiencies of the conventional SPM machines are almost constant for all the investigated airgap

lengths for both 3MW and 10MW, as shown in TABLE VII. However, the SPM-V machines show a considerable drop in efficiency towards larger airgap length and higher pole numbers ($\bar{\tau}_r \leq 2.2$), as shown in Fig. 21. This trend is very similar to that shown for the 3kW machines.

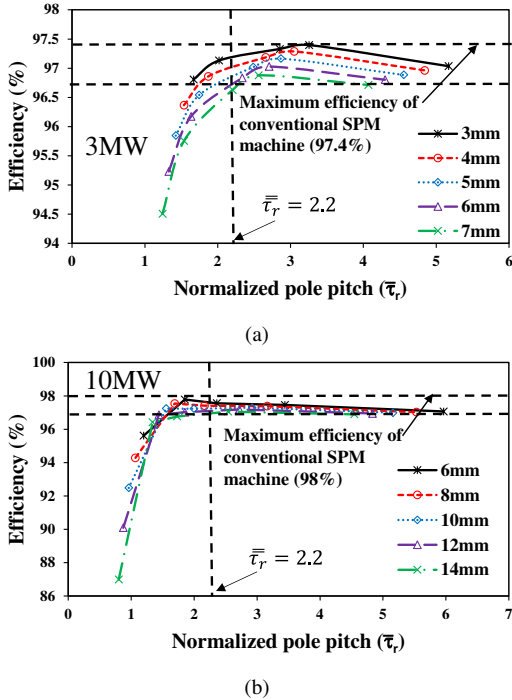


Fig. 21. Comparison of efficiency for the SPM-V machines as a function of ($\bar{\tau}_r$). (a) 3MW and (b) 10MW.

However, it is observed that at multi-MW power levels, the efficiencies of the SPM-V machines are either comparable to or lower than their conventional counterparts. This is largely due to their higher electromagnetic losses compared to the conventional SPM machines, as shown in Fig. 22.

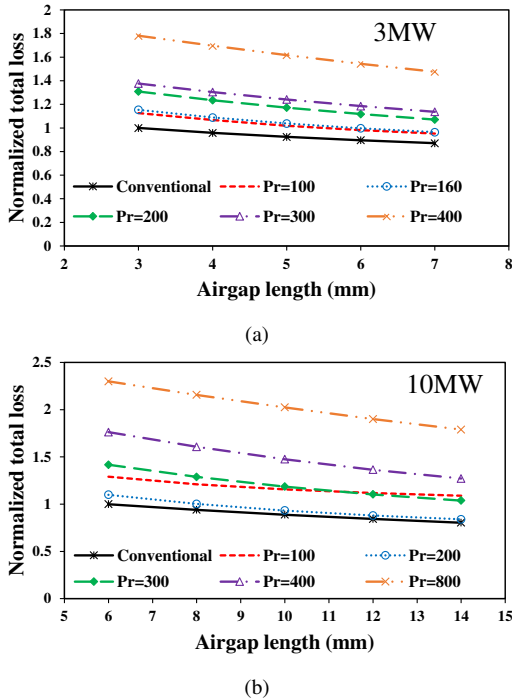


Fig. 22. Comparison of normalized total losses for different airgap lengths between the conventional SPM and SPM-V machines with different slot/pole numbers. (a) 3MW. (b) 10MW. Conventional SPM machines with 3mm and 6mm airgap lengths are taken as reference for the calculation of normalized values for 3MW and 10MW, respectively.

Unlike the 3kW machines [Fig. 15(b)], the losses of 3MW and 10MW SPM-V machines are always higher than the conventional counterpart across all investigated pole numbers and airgap lengths. However, when $\bar{\tau}_r > 2.2$, a reasonably good efficiency can still be achieved for the multi-MW SPM-V machines, as shown in Fig. 21.

D. Demagnetization

The demagnetization analyses, similar to the 3kW machines, have been performed under 3-phase symmetric short-circuit fault. It is observed that at multi-MW power levels, both the conventional SPM and SPM-V machines are likely to be irreversibly demagnetized because of their high electrical loading.

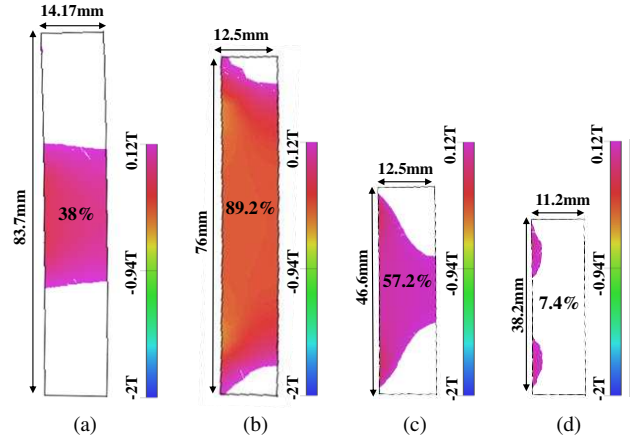


Fig. 23. Flux density distributions in the magnets for the 3MW machine with 3mm airgap length at the instant of peak d -axis short-circuit current. (a) Conventional SPM machine. SPM-V machines with (b) $P_r=100$, (c) $P_r=160$ and (d) $P_r=200$. The dimensions of the magnets and the percentage of irreversibly demagnetized area (coloured) are also highlighted.

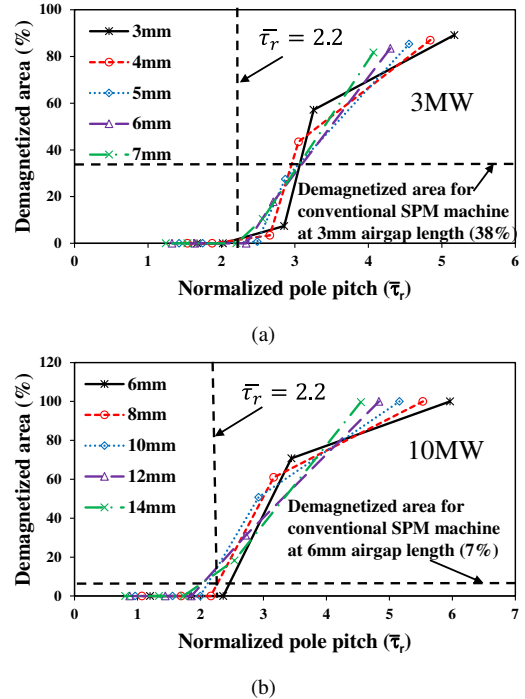


Fig. 24. Percentage of 'demagnetized area' in the magnets (the one exposed to maximum demagnetization) as a function of normalized pole pitch ($\bar{\tau}_r$) for SPM-V machines. (a) 3MW and (b) 10MW.

As an example, the 3MW conventional SPM and SPM-V machines with 3mm airgap length have been selected. The flux density distribution within one magnet that suffers the highest demagnetization due to peak d -axis short-circuit flux is shown in Fig. 23. The flux density below the knee point

(0.12T), i.e. the ‘demagnetized area’, is represented using a colour map. It is worth noting that this is the smallest investigated airgap length for the 3MW power level and therefore the risk of demagnetization is expected to be maximum. It can be observed that there is a higher risk of irreversible demagnetization towards lower pole numbers for the SPM-V machines ($P_r=100$ and $P_r=160$). This is due to their large coil inductance [14]. The SPM-V machines with higher pole numbers are less likely to be demagnetized, and their demagnetized area is even smaller than that of the conventional SPM machines.

The ‘demagnetized area’ as a function of $\overline{\tau}_r$ for the 3MW and 10MW SPM-V machines are shown in Fig. 24. It is found that the demagnetization risk starts to emerge at $\overline{\tau}_r \geq 2.5$ and becomes more serious (>50%) beyond $\overline{\tau}_r = 3$ for both 3MW and 10MW SPM-V machines. Although, $\overline{\tau}_r \geq 2.2$ is a good design point for achieving an overall good performance for the SPM-V machines, special consideration needs to be given to avoid any potential irreversible demagnetization risk.

VI. CONCLUSION

The performance comparison between the SPM-V and conventional SPM machines with different power ratings and airgap lengths has been carried out in this paper. The study shows that at 3kW power level and with a relatively low electrical loading (~9.3AT/mm), the SPM-V machines designed with normalized pole pitch $\overline{\tau}_r > 2.2$ can outperform the conventional SPM machines with higher torque density and efficiency, lower torque ripple and comparable power factor (~0.9). However, at multi-MW power levels such as 3MW and the 10MW investigated in this paper, the power factors of the SPM-V machines drop significantly to a low range (~0.4-0.55). Also, the efficiencies become comparable to or lower than those of the conventional counterpart. Nevertheless, the study revealed that for all power levels, $\overline{\tau}_r = 2.2$ is a good threshold, beyond which the SPM-V machines can exhibit a performance closest to their optimal capability. However, with $\overline{\tau}_r > 2.2$, the multi-MW SPM-V machines are prone to the potential risk of irreversible demagnetization and hence require special consideration.

REFERENCES

- [1] Y. Yuan, W. Meng, X. Sun, and L. Zhang, “Design optimization and analysis of an outer-rotor direct-drive permanent-magnet motor for medium-speed electric vehicle,” *World Electr. Veh. J.*, vol. 10, p. 16, 2019.
- [2] F. Jin, J. Si, Z. Cheng, P. Su, L. Dong, and G. Qi, “Analysis of a six-phase direct-drive permanent magnet synchronous motor with novel toroidal windings,” in *2019 IEEE Veh. Pow. and Prop. Conf. (VPPC)*, Oct. 2019, pp. 1–6.
- [3] W. Gul, Q. Gao, and W. Lenwari, “Optimal design of a 5-MW double-stator single-rotor PMSG for offshore direct drive wind turbines,” *IEEE Trans. Ind. Appl.*, vol. 56, no. 1, pp. 216–225, Jan. 2020.
- [4] A. Chowdhury and Y. Sozer, “Design and analysis of a hook shaped stator core with ring winding transverse flux machine for wind turbine applications,” in *2020 IEEE Energy Conversion Congress and Exposition (ECCE)*, 2020, pp. 540–544.
- [5] M. Chen, L. Huang, P. Tan, Y. Li, G. Ahmad, and M. Hu, “A stator-PM transverse flux permanent magnet linear generator for direct drive wave energy converter,” *IEEE Access*, vol. 9, pp. 9949–9957, 2021.
- [6] M. A. Baig, J. Ikram, A. Iftikhar, S. S. H. Bukhari, N. Khan, and J.-S. Ro, “Minimization of cogging torque in axial field flux switching machine using arc shaped triangular magnets,” *IEEE Access*, vol. 8, pp. 227193–227201, 2020.
- [7] O. Dobzhanskyi, E. Hossain, E. Amiri, R. Gouws, V. Grebenikov, L. Mazurenko, M. Pryjmak, and R. Gamaliia, “Axial-flux PM disk generator with magnetic gear for oceanic wave energy harvesting,” *IEEE Access*, vol. 7, pp. 44813–44822, 2019.
- [8] A. B. Kjaer, S. Korsgaard, S. S. Nielsen, L. Demsa, and P. O. Rasmussen, “Design, fabrication, test, and benchmark of a magnetically geared permanent magnet generator for wind power generation,” *IEEE Trans. on Energy Convers.*, vol. 35, no. 1, pp. 24–32, 2020.
- [9] J. Li, K. T. Chau, J. Z. Jiang, C. Liu, and W. Li, “A new efficient permanent-magnet vernier machine for wind power generation,” *IEEE Trans. Magn.*, vol. 46, no. 6, pp. 1475–1478, Jun. 2010.
- [10] D. K. Jang and J. H. Chang, “Design of a Vernier machine with PM on both sides of rotor and stator,” *IEEE Trans. Magn.*, vol. 50, no. 2, Feb. 2014.
- [11] Y. Gao, R. Qu, D. Li, and F. Chen, “Force ripple minimization of a linear vernier permanent magnet machine for direct-drive servo applications,” *IEEE Trans. Magn.*, vol. 53, no. 6, pp. 1–5, 2017.
- [12] D. K. Kana Padinharu, G. J. Li, Z. Q. Zhu, M. P. Foster, D. A. Stone, A. Griffio, R. Clark, and A. Thomas, “Scaling effect on electromagnetic performance of surface mounted permanent magnet Vernier machine,” *IEEE Trans. Magn.*, vol. 56, no. 5, pp. 1–15, May 2020.
- [13] H. Polinder, D. Bang, R. P. J. O. M. van Rooij, A. S. McDonald, and M. A. Mueller, “10 MW wind turbine direct-drive generator design with pitch or active speed stall control,” in *Proc. IEEE Int. Conf. Electr. Mach. Drives*, Antalya, 2007, vol. 2, pp. 1390–1395.
- [14] D. K. Kana Padinharu, G. J. Li, Z. Q. Zhu, M. P. Foster, D. A. Stone, A. Griffio, M. Odavic, R. Clark, and A. Thomas, “Influence of demagnetization on selecting the optimum slot/pole number combination for 3MW surface mounted permanent magnet Vernier machine,” in *Proc. 22nd Int. Conf. Electr. Mach. Syst. (ICEMS)*, Harbin, China, Aug. 2019, pp. 1–6.
- [15] S. Hyoseok, N. Niguchi, and K. Hirata, “Characteristic analysis of surface permanent-magnet Vernier motor according to pole ratio and winding pole number,” *IEEE Trans. Magn.*, vol. 53, no. 11, Nov. 2017.
- [16] L. Wu, R. Qu, D. Li, and Y. Gao, “Influence of pole ratio and winding pole numbers on performance and optimal design parameters of surface permanent-magnet Vernier machines,” *IEEE Trans. Ind. Appl.*, vol. 51, no. 5, pp. 3707–3715, Sep. 2015.
- [17] M. Choi and B. Kim, “Calculation of PM Vernier motors using an improved air-gap permeance function,” *IEEE Trans. Magn.*, vol. 55, no. 6, pp. 1–5, 2019.
- [18] D. K. Kana Padinharu, G. J. Li, Z. Q. Zhu, Z. Azar, R. Clark, and A. Thomas, “Effect of airgap length on electromagnetic performance of surface mounted permanent magnet Vernier machine,” in *2020 Int. Conf. Electr. Mach. (ICEM)*, 2020, vol. 1, pp. 1882–1888.
- [19] D. W. Li, R. H. Qu, J. Li, L. Y. Xiao, L. L. Wu, and W. Xu, “Analysis of torque capability and quality in Vernier permanent-magnet machines,” *IEEE Trans. Ind. Appl.*, vol. 52, no. 1, pp. 125–135, Jan. 2016.
- [20] A. Toba and T. A. Lipo, “Generic torque-maximizing design methodology of surface permanent-magnet Vernier machine,” *IEEE Trans. Ind. Appl.*, vol. 36, no. 6, pp. 1539–1546, Nov. 2000.
- [21] K. Xie, D. Li, R. Qu, X. Ren, M. R. Shah, and Y. Pan, “A new perspective on the PM Vernier machine mechanism,” *IEEE Trans. Ind. Appl.*, vol. 55, no. 2, pp. 1420–1429, 2019.
- [22] D. K. Kana Padinharu, G. J. Li, Z. Q. Zhu, R. Clark, Z. Azar, and A. Thomas, “Investigation of scaling effect on power factor of permanent magnet Vernier machines for wind power application,” *IET Electric Power Applications*, vol. 14, no. 11, pp. 2136–2145, Jul. 2020.
- [23] L. R. Huang, J. H. Feng, S. Y. Guo, J. X. Shi, W. Q. Chu, and Z. Q. Zhu, “Analysis of torque production in variable flux reluctance machines,” *IEEE Trans. on Energy Convers.*, vol. 32, no. 4, pp. 1297–1308, Dec. 2017.
- [24] Z. Q. Zhu and D. Howe, “Influence of design parameters on cogging torque in permanent magnet machines,” *IEEE Trans. Energy Convers.*, vol. 15, no. 4, pp. 407–412, Dec. 2000.
- [25] Y. Oner, Z. Q. Zhu, and W. Chu, “Comparative study of Vernier and interior PM machines for automotive application,” in *Proc. IEEE Vehicle Power and Propulsion Conf.*, Hangzhou, China, Oct. 2016, pp. 1–6.
- [26] Z. S. Du and T. A. Lipo, “Torque performance comparison between a ferrite magnet vernier motor and an industrial interior permanent magnet machine,” *IEEE Trans. Ind. Appl.*, vol. 53, no. 3, pp. 2088–2097, May 2017.
- [27] L. Wu, R. Qu, and D. Li, “Analysis of eddy current losses in surface-mounted permanent magnet vernier machines,” in *Proc. IEEE Int. Conf. Electr. Mach. Drives*, May 2017, pp. 1–6.
- [28] J. Zhang, A. Tounzi, P. Delarue, F. Piriou, V. Leontidis, A. Dazin, G. Caignaert, and A. Libaux, “Quantitative design of a high performance permanent magnet Vernier generator,” *IEEE Trans. Magn.*, vol. 53, no. 11, Nov. 2017.

- [29] K. F. Xie, D. W. Li, R. H. Qu, and Y. T. Gao, "A novel permanent magnet vernier machine with Halbach array magnets in stator slot opening," *IEEE Trans. Magn.*, vol. 53, no. 6, Jun. 2017.
- [30] D. K. Kana Padinharu, G. J. Li, Z. Q. Zhu, R. Clark, A. S. Thomas, and Z. Azar, "System-level investigation of multi-MW direct-drive wind power PM Vernier generators," *IEEE Access*, vol. 8, pp. 191433–191446, 2020.
- [31] H. Polinder, F. F. A. van der Pijl, G.- de Vilder, and P. J. Tavner, "Comparison of direct-drive and geared generator concepts for wind turbines," *IEEE Trans. Energy Convers.*, vol. 21, no. 3, pp. 725–733, Sep. 2006.
- [32] J. R. Hendershot and T. J. E. Miller, *Design of brushless permanent-magnet motors*. Hillsboro, OH: Magna Pysics, 1994.